CRACK MECHANISMS AND CRACK INTER-ACTION IN THIN FILMS

Mechanical Engineering
Technical Report ME-TR-1

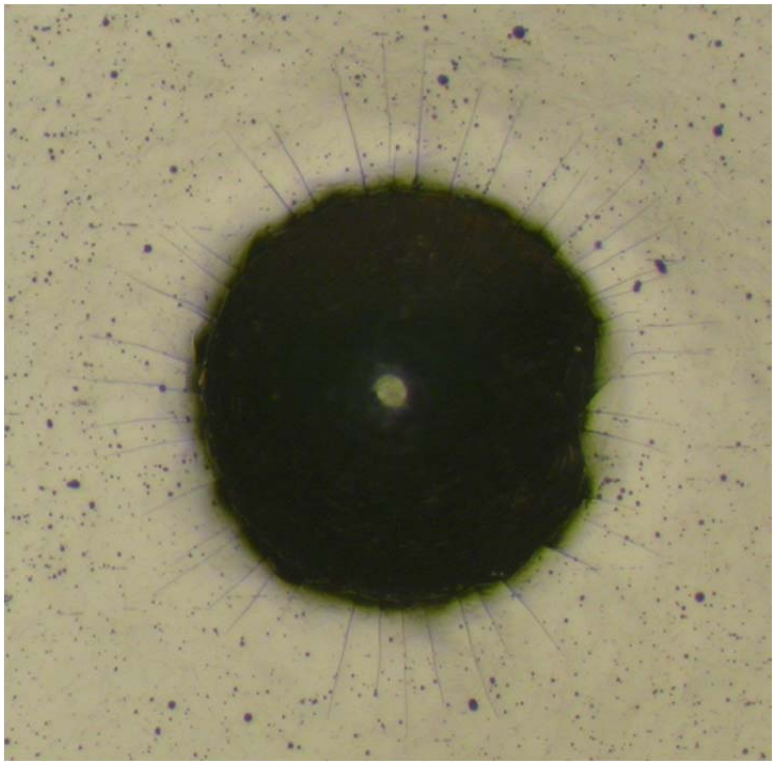

AARHUS
UNIVERSITY
DEPARTMENT OF ENGINEERING

DATA SHEET

Title: Crack Mechanisms and Crack Interaction in Thin Films
Subtitle: Mechanical Engineering
Series title and no.: Technical report ME-TR-1

Authors: Mads Krabbe
Department of Engineering – Mechanical Engineering, Aarhus University

Internet version: The report is available in electronic format (pdf) at the Department of Engineering website http://www.eng.au.dk.

Publisher: Aarhus University©
URL: http://www.eng.au.dk

Year of publication: 2012 Pages: 34
Editing completed: April 2012

Abstract: The report contains a description of the theory for through-surface channeling crack in thin film systems. Key topics and mechanisms are described including channeling criteria, crack interaction and elastic mismatch in the system. A case of radial cracks spreading from a Rockwell indenter is used to describe how the theory can be used to determine fracture toughness and residual stresses in a thin film.

Keywords: Thin films, fracture mechanics, channeling cracks, steady-state cracking, elastic mismatch, crack interaction, crack spacing, indentation fracture toughness, Rockwell indentation.

Supervisor: Henrik Myhre Jensen
Financial support: Forskningsrådet for Teknologi og Produktion

Please cite as: Mads Krabbe, 2012. Crack Mechanisms and Crack Interaction in Thin Films. Department of Engineering, Aarhus University. Denmark. 34 pp. - Technical report ME -TR-1

Cover photo: Nis Dam Madsen, iNANO, Aarhus University

ISSN: 2245-4594

CRACK MECHANISMS AND CRACK INTERACTION IN THIN FILMS

Mads Krabbe

Aarhus University, Department of Engineering

Abstract

The report contains a description of the theory for through-surface channeling crack in thin film systems. Key topics and mechanisms are described including channeling criteria, crack interaction and elastic mismatch in the system. A case of radial cracks spreading from a Rockwell indenter is used to describe how the theory can be used to determine fracture toughness and residual stresses in a thin film.

Contents

Chapter 1

Introduction

Hard coatings can be applied on materials to enhance their mechanical properties. The coatings can be applied on e.g. cutting tools which can be coated to enhance wear resistance on gears and bearings to reduce friction and enhance life.

In this project, focus is on developing methods to link microstructural characterisation with measurements and calculations of the coating system including the mechanical and especially the fracture mechanical properties. The mechanical data will be obtained by nano-indentation which yield hardness, Young's modulus and possibly creep. By comparing nano-indentation data with theoretical fracture mechanical models, quantitative values of fracture toughness are obtained.

To understand the wear properties of a coating, it is of paramount importance to know both the hardness and the fracture toughness. In the project, it is of key interest to establish a link between the mechanical and fracture mechanical properties and the wear resistance of the coating. It is a hypothesis, which will be pursued in this project that the wear resistance of such coatings is linked to the crack pattern which forms in the coating during indentation, and that the parameters governing this pattern thus can be used to optimise the performance of the coatings. This general hypothesis will then be used in particular to develop and optimise the properties of the coatings.

This assignment is composed while the work is in progress and is not in the final form. A number of fracture mechanical models for coatings have been studied. A selected number of basic models for crack propagation is presented along with one case of special interest.

Chapter 2

Single channelling crack

2.1 Basic mechanisms and expressions

A brittle coating under homogenous tensile stress may fail by the extension of channelling cracks. consider the 3D crack in figure 2.1. The crack is a through-thickness crack in a film reaching all the way through the film to the substrate. The film is loaded by a uniaxial tensile stress σ. The film thickness is denoted h. When the crack reaches a certain length, the energy

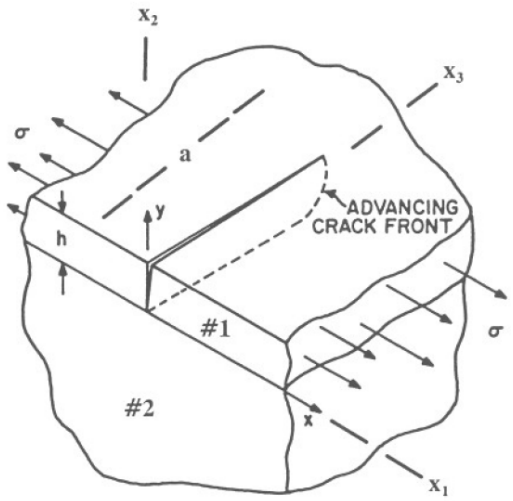

Figure 2.1: A 3D through-crack channelling across a film [1]

release rate for the crack growth becomes independent of the crack length and conditions at the crack tip. The crack growth has then reached steady state growth. Xia and Hutchinson, [2], amongst others cites the results from Nakumura and Kamath [3] who investigated the three-dimensional crack growth. The results from this paper states that the crack reaches steady-state when the crack length is only a few times larger than the film thickness, see figure 2.2. This results is also confirmed by [2] who has

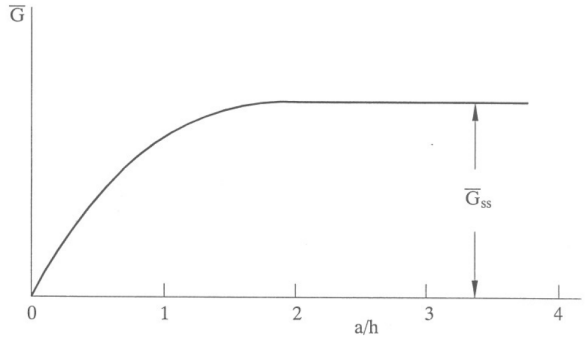

Figure 2.2: Qualitative approach to steady-state channelling. [1] based on results from [3]

made a two-dimensional analysis of through-thickness cracks in thin films. For elastic identical film and substrate, [2] concludes that steady-state is reached for $a/h \approx 4$ (a is the crack length) for a central crack. The investigation performed by [3] investigates only the case with an infinitely stiff substrate. Newer results performed by Ambrico and Begley [4] investigates the propagation of a crack from an initial flaw towards steady-state crack growth for a through-thickness crack. The analysis is a three-dimensional finite-element analysis. Contrary to [3], Ambrico and Begley also investigates the effects of the elastic properties for the substrate. The results can be seen i figure 2.3. The elastic mismatch between the film and the substrate is described with the parameter α which is explained in detail in section 2.2. Shortly, $\alpha = -1$ corresponds to an infinitely stiff substrate and α increases with the relative film stiffness. for an infinitely stiff film, $\alpha = 1$. The original result from Nakamura and Kamath can be seen in the top left corner of the two figures for $\alpha = -1$ where it can be seen that steady-state is obtained for a crack length only a few times the film thickness. When α increases the steady-state length increases too. For $\alpha = 0$ which is a system

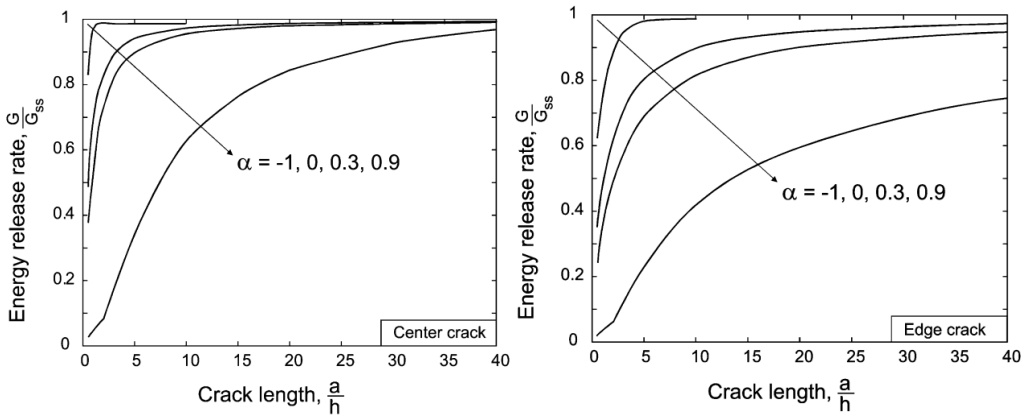

(a) Center cracks (b) Edge cracks

Figure 2.3: Energy release rate for elastic cracks i a single layer vs channelling crack length for different material mismatch

with identical elastic properties for the film and substrate, the steady-state length is much longer. For an edge crack, an energy release rate of 90% is first obtained when the crack length is 15 times the film thickness.

In steady state cracking, the energy release rate can be evaluated without knowledge of the conditions at the crack front and the shape of the crack front. To obtain the energy release rate, two plane problems are examined. The strain energy in a unit slice far behind the crack front is subtracted from the strain energy far ahead. One solution formula to this problem is

$$G_{ss} = \frac{\sigma}{2h} \int_0^h \delta(y) dy \tag{2.1}$$

Where $\delta(y)$ is the displacement profile for a plane strain crack and σ is the film stress. An alternative formula is

$$G_{ss} = \frac{1}{h} \int_0^h G(a) da \tag{2.2}$$

Where $G(a)$ is the energy release rate of a plane strain crack of depth a, see figure 2.4 [5]. If the system is elastic homogenous the corresponding plane strain problem is an edge crack in a half plane. This is a standard fracture mechanics problem and the solution is $G(a) = 3,952\sigma^2 \frac{a}{E}$ [6]. If

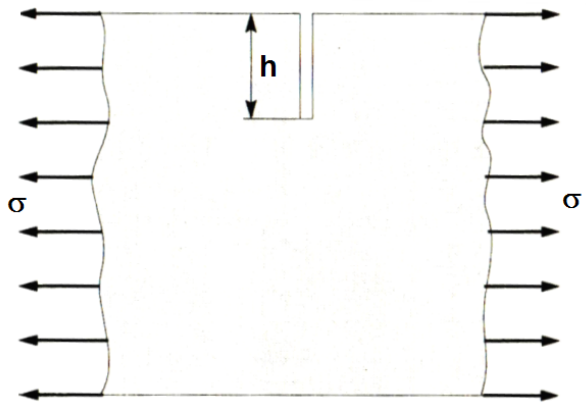

Figure 2.4: Edge crack in a half plane

this expression is inserted in equation 2.2 the result is

$$G_{ss} = 1,976\sigma^2 \frac{h}{\bar{E}} \tag{2.3}$$

2.2 elastic mismacth

The above expressions are only valid for an elastic homogenous film-substrate system. For system with different elastic properties for the film and substrate the situation is more complicated. To describe the elastic mismatch, the two Dundurs' parameters are used [7]

$$\alpha = \frac{k(\kappa_1 + 1) - (\kappa_2 + 1)}{k(\kappa_1 + 1) + (\kappa_2 + 1)}, \quad \beta = \frac{k(\kappa_1 - 1) - (\kappa_2 - 1)}{k(\kappa_1 + 1) + (\kappa_2 + 1)} \tag{2.4}$$

Where:
k is the ratio of the shear moduli, $k = \frac{S_1}{S_2}$.
$\kappa = 3 - 4\nu$ for plane strain and $\kappa = \frac{3-\nu}{1+\nu}$ for plane stress.
The indices 1 and 2 refers to respectively the film and the substrate.
If the above expressions for k and κ are inserted in equations 2.4, the expression for α and β for plane strain is [8]

$$\alpha = \frac{\bar{E}_f - \bar{E}_s}{\bar{E}_f + \bar{E}_s}, \quad \beta = \frac{1}{2}\frac{\bar{E}_s \frac{1-2\nu_f}{1-\nu_f} - \bar{E}_f \frac{1-2\nu_s}{1-\nu_s}}{\bar{E}_f + \bar{E}_s} \tag{2.5}$$

Where the subscript f and s denotes the film and substrate respectively. $\bar{E} = \frac{E}{1-\nu^2}$ is the plane strain tensile modulus. From equation 2.4 it is apparent that α can vary from -1 to +1. $\alpha = -1$ is one limit case with an infinitely stiff substrate an compliant film and $\alpha = 1$ is for an infinitely stiff film and compliant substrate. Since k in equation 2.4 is positive ν is required to be in the range $0 \leq \nu \leq \frac{1}{2}$. The physically admissible range for β with respect to α is then restricted to $|\alpha - 4\beta| \leq 1$. For most practical material combinations, the value of β typically lies between $\beta = 0$ and $\beta = \alpha/4$. Furthermore, β typically has only little influence on the results compared to the influence from α. For that reason, results are typically only presented for the two limiting values of β, $\beta = 0$ and $\beta = \alpha/4$ [9].

Beuth [9] has developed the approach issued by Hutchinson and Sou [5] to account for elastic mismatch. Beuth presents solutions to two problems. One is the fully cracked problem and the second is a partially cracked film. Only the fully cracked case is described.

[9] determines the mode I stress intensity factor K_I for the fully cracked problem with the crack tip at the interface. A sketch of the problem can be seen in figure 2.5. For the fully cracked problem Beuth defines K_I as

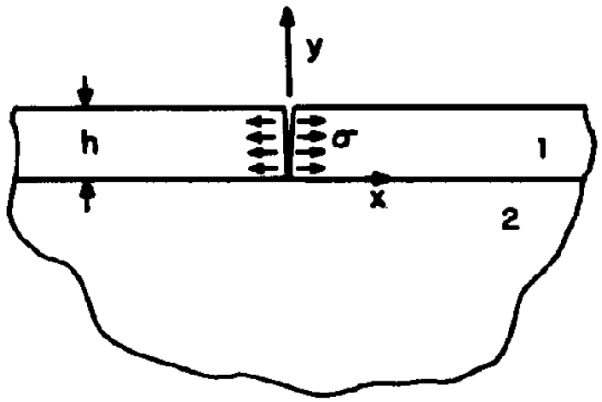

Figure 2.5: Crack problem investigated by Beuth [9]

$$K_I \equiv \lim_{y \to 0^-} \left[(-2\pi y)^s \sigma_{xx}(0, y) \right] \tag{2.6}$$

The stress singularity exponent s is a function of the Dundurs parameters α and β and s satisfies the following equation derived by Zak and Williams

[10]:

$$\cos(s\pi) - 2\frac{\alpha-\beta}{1-\beta}(1-s)^2 + \frac{\alpha-\beta^2}{1-\beta^2} = 0 \tag{2.7}$$

No elastic mismatch between film and substrate giving $\alpha = 0$ and $\beta = 0$ gives $s = 1/2$ and equation 2.7 corresponds to the classic definition of the mode I stress intensity factor for a crack in a homogenous solid. The stresses just ahead of the crack tip in the y direction is given by

$$\sigma_{xx}(0, y) = C_1 \frac{\sigma h^s}{(-y)^s} \tag{2.8}$$

Where C_1 is a nondimensional function of α and β only. The detailed derivation of K_I and σ_{xx} is not given here.

To describe the steady state energy release rate, Beuth introduces the non-dimensional quantity $g(\alpha, \beta)$

$$g(\alpha, \beta) = \frac{\int_0^h \delta(y)dy}{\pi \frac{\sigma}{E_f}} h^2 \tag{2.9}$$

g is a nondimensionalised integral of the crack opening displacement and is a function of the two Dundur's parameters. A plot of $g(\alpha, \beta)$ as a function of α can be seen in figure 2.6. The steady state energy release rate for a

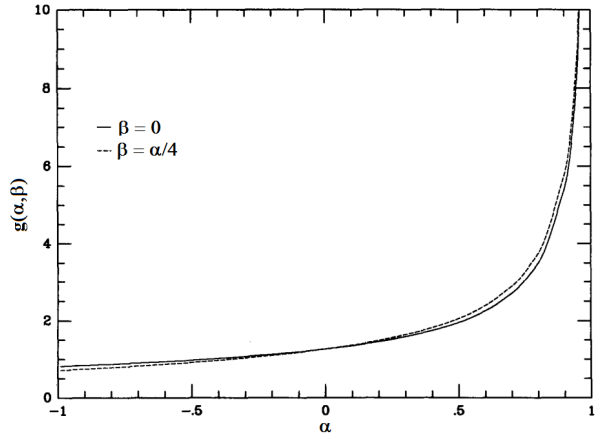

Figure 2.6: Plot of $g(\alpha, \beta)$ as a function of α for $\beta = 0$ and $\beta = \alpha/4$

through-thickness channelling crack can then be expanded with $g(\alpha, \beta)$ to

account for elastic mismatch. The argument from equation 2.1 can then be used to give the expression for the steady-state energy release rate for a through-thickness channelling crack for elastic mismatch.

$$\begin{aligned} G_{ss} &= \frac{\sigma}{2h}\int_0^h \delta(z)dz = \frac{\sigma}{2h} g(\alpha,\beta)\frac{\pi h^2 \sigma}{\bar{E}_f} \\ &= \frac{1}{2}\frac{\sigma^2 h}{\bar{E}_f}\pi g(\alpha,\beta) \end{aligned} \tag{2.10}$$

Looking at elastically identical materials, it is recalled from equations 2.1 and 2.2 that the steady state energy release rate can be expressed in two ways:

$$G_{ss} = \frac{\sigma}{2h}\int_0^h \delta(z)dz, \quad G_{ss} = \frac{1}{h}\int_0^h G(a)da \tag{2.11}$$

Equating these two expressions and inserting $\int_0^h \delta(y)dy = g(\alpha,\beta)\pi\sigma h^2/\bar{E}_f$ from equation 2.9 and remembering that for linear elastic fracture mechanics $G = K_I^2/\bar{E}_f$ the following expression is derived

$$g(0,0) = 1,1215^2 \tag{2.12}$$

It is used that for an edge crack in an homogenous half-plane $K_I = 1,1215\sigma\sqrt{\pi a}$ [6] . Inserting this value for $g(0,0)$ in equation 2.11 gives $G_{ss} = 1,976\frac{\sigma^2 h}{\bar{E}_f}$, which is the same as equation 2.2 from [5].

Chapter 3

Multiple cracks and crack interaction

When gradually increasing the stress in a film attached to a substrate and given that the interface fracture toughness is high enough to prevent delamination, the film will fail by the formation of a number of cracks propagating from the surface to the interface and subsequent channelling across the film.

A number of different models for the interaction and saturation of parallel channelling cracks has been set up.

3.1 Crack interaction and crack spacing

Thouless [11] carried out an analysis for parallel cracking of a system with identical elastic properties of film and substrate. The cracks are assumed to be propagating simultaneously and have obtained steady-state.

The procedure to determine the energy release rate is the same as presented by Hutchinson and Suo [5]. The energy release rate is obtained by comparing the strain energy stored in a unit slice far ahead and far behind the front of parallel propagating cracks. As for the single crack this can be found by integrating a text book solution for an array of edge cracks, see figure 3.1.

$$G_{ss} = \frac{1}{h}\int_0^h G(y)dy \tag{3.1}$$

Where $G(y)$ is the energy release rate for one crack for the problem in

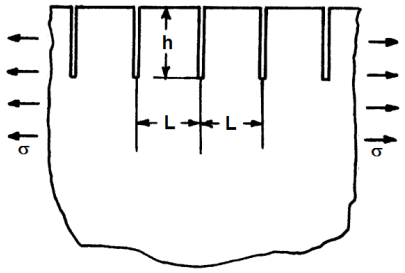

Figure 3.1: Fracture-mechanical problem used to compute the energy release rate [6]

figure 3.1. The solution to the integral is.

$$G_{ss} \approx 1,98\frac{\sigma^2 h}{\bar{E}_f} \quad L \gtrsim 8h$$
$$G_{ss} \approx \left[0,5\frac{l}{h} - 0,0316\left(\frac{l}{h}\right)^2\right]\frac{\sigma^2 h}{E} \quad L \lesssim 8h \tag{3.2}$$

It can be seen in equation 3.2 that for a crack spacing larger than $8h$ the cracks do not interact.

If the stress in the film is gradually increased, then, according to Thouless, an array of cracks will form when a critical stress is reached. This critical stress can be found by isolating σ in the first line in equation 3.2. The spacing of these initial cracks will be determined by the position of any existing flaws in the film but it will be larger than $8h$. If the stress is larger than this critical stress, minimum crack spacing will be given from isolating L/h in the second line in equation 3.2.

$$\frac{\lambda}{h} \approx 8\left(1 - \sqrt{1 - 0,5\left(\frac{\Gamma_f E}{\sigma^2 h(1-\nu^2)}\right)^2}\right) \tag{3.3}$$

Where Γ_f is the fracture toughness, the critical energy release rate for the film. Note that this is a minimum crack spacing, the actual crack spacing may differ from this. The λ notation is used to emphasise that this is a material value for the specific film.

Hutchinson and Suo [5] uses the same argument as Thouless [11] to investigate the energy release rate for an array of cracks.

Hutchinson and Suo develops this approach to consider not only the simultaneously propagation of an array of cracks. Consider a situation where a film is already cracked due to a certain loading σ. If the loading is increased, a new set of cracks is nucleated and propagates halfway between the existing cracks. The energy release rate for this new set of cracks can be computed with the same argument as used when calculating the energy release rate for a single crack. The strain energy far ahead and far behind the crack front for the new set of cracks is used to calculate the energy release rate for the new set of cracks. The strain energy in a unit slice containing one "old" and two "new" cracks is considered. Far behind the crack tip the crack spacing is L and there are two "new" cracks. Far ahead the crack tip there is one "old" crack with a spacing $2l$. Denoting the strain energy behind the crack tip U_l and the strain energy ahead of the crack tip U_{2l} the energy release rate can be calculated as

$$G_{ss,seq} = (2U_l - U_{2l})\frac{1}{h} \tag{3.4}$$

Inserting the solution from equation 3.2 for G_{ss} for the simultaneously propagation the following expression for sequential propagation is derived.

$$\begin{aligned} G_{ss,seq} &= (2U_l - U_{2l})\frac{1}{h} \\ &= 2\left[0,5\frac{L}{h} - 0,0316\left(\frac{L}{h}\right)^2\right]\frac{\sigma^2 h}{\bar{E}_f} - \left[0,5\frac{2L}{h} - 0,0316\left(\frac{2L}{h}\right)^2\right]\frac{\sigma^2 h}{\bar{E}_f} \\ &= 2 \cdot 0,0316\left(\frac{L}{h}\right)^2\frac{\sigma^2 h}{\bar{E}_f} \end{aligned} \tag{3.5}$$

Delannay and Warren [12] has carried out an analysis much similar to the above.

Thouless et. al. [13] uses a different argument to look at the crack spacing than originally posted by Thouless [13]. Thouless et. al. uses an energy argument to derive an equilibrium crack spacing. The strain energy in the uncracked film is

$$U_0 = 0.5\frac{\sigma^2 h}{\bar{E}_f} \tag{3.6}$$

Using the result from equation 3.2 which gives the energy difference between the cracked and uncracked film, the strain energy in the cracked film can

be found to be

$$U_l = 0,0316\frac{L}{h}\frac{\sigma^2 h}{\bar{E}_f} \tag{3.7}$$

The critical energy release rate Γ_f and the energy associated with the crack array can be related by

$$U_c = \Gamma_f \frac{h}{L} \tag{3.8}$$

The energy equilibrium crack spacing must then be when the total energy of the film is minimised. The total energy can be expresses as

$$U_{total} = U_l + U_c = 0,0316\frac{L}{h}\frac{\sigma^2 h}{\bar{E}_f} + \Gamma_f \frac{h}{L} \tag{3.9}$$

The minimal total energy can the be found by finding the minimum for the expression in equation 3.9

$$\begin{aligned} \frac{\partial U_l}{\partial L} + \frac{\partial U_c}{\partial L} &= 0 \Rightarrow \\ 0,0316\frac{\sigma^2 h}{\bar{E}_f}\frac{1}{h} - \frac{\Gamma_f h}{L^2} &= 0 \Rightarrow \\ \frac{\lambda_{equlibrium}}{h} &= \sqrt{0,0316^{-1}}\sqrt{\frac{\bar{E}_f \Gamma_f}{\sigma^2 h}} \\ &\approx 5,6\sqrt{\frac{\bar{E}_f \Gamma_f}{\sigma^2 h}} \end{aligned} \tag{3.10}$$

This expression gives a larger spacing for the same film properties than the expression stated in equation 3.3 which is the thermodynamically smallest possible spacing. The argument from equation 3.5 gives a spacing intermediate to these two. Another interesting difference is that equation 3.3 predicts that the absolute crack spacing L should decrease for increasing film thickness h. Equation 3.10 on the contrary states that L increases as $\sqrt{h}$. [13] confirms the latter relation by experiments.

3.1.1 Elastic mismatch

Xia and Hutchinson [2] have presented a solution for the driving force for propagation of parallel cracks in an elastic inhomogenous system. To implement the elastic mismatch, a characteristic length l is introduced

$$l \equiv \frac{\pi}{2} g(\alpha, \beta) h \tag{3.11}$$

Where $g(\alpha, \beta)$ is the nondimensional factor describing the elastic mismatch introduced my Beuth, [9], see section 2.2. For an elastic homogenous system, $l = 1.976h$. By the use of the factor l, the energy release rate for the simultaneous propagation of a crack array can be expressed as

$$G_{ss} = \frac{l\sigma^2}{\bar{E}_f} \tanh\left(\frac{L}{2l}\right) \tag{3.12}$$

Like the expression developed by [11], equation 3.2, the expression approaches that for a single crack when the crack spacing is increased. When $L = 3l$, the value for G_{ss} is 90% of the value for an isolated crack. In [11], the value for G_{ss} for a crack array equals the result for a single crack when $L = 8h$. For $L = 8h$ and elastically identical materials, $\tanh\left(\frac{L}{2l}\right) = 0,97$. The crack interaction distance depends on the elastic mismatch coefficient $g(\alpha, \beta)$. For stiff substrates, the elastic mismatch has a strong influence on the crack interaction distance. Figure 3.2 shows a plot of $Lh_{singlecrack}$ as a function of the elastic mismatch parameter α. $Lh_{singlecrack}$ is the crack spacing at which G_{ss} for the parallel array of cracks has reached 97% of the value for a single crack, i.e. the value $\frac{L}{h} = 8$ from [11] for elastic identical materials. Figure 3.2 shows that when the film is very stiff compared to the

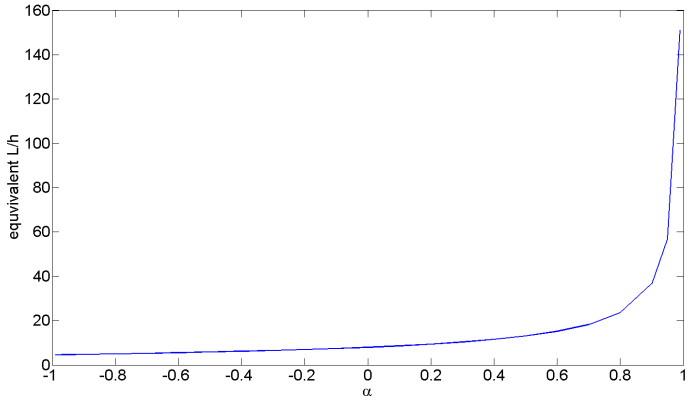

Figure 3.2: Crack spacing for no interaction for varying α

substrate the interaction distance increases drastically. Using the argument from [5], equation 3.4, the energy release rate for the sequential propagation of cracks cans be expressed as [2]

$$
\begin{aligned}
G_{ss} &= 2 \cdot G_{ss,L} - G_{ss,2L} \\
&= \frac{l\sigma^2}{\bar{E}_f}\left[2\tanh\left(\frac{L}{2l}\right) - \tanh\left(\frac{L}{l}\right)\right]
\end{aligned} \tag{3.13}
$$

3.1.2 Yielding substrate

If the substrate is ductile, the crack spacing is dictated by the substrate yield stress. The crack spacing for a yielding substrate can be approximated by a simple shear lag analysis. The shear lag analysis is described by Hu and Evans [14] and Agrawal and Raj [15]. The procedure is also described by Beuth and Klingbeil [16]. The concept of the shear lag model is that the substrate yields at the surface. This results in a shear yield stress τ being transferred to the film from the substrate. Hu and Evans [14] suggests a constant shear stress. It is assumed that a crack exist in the film. At the crack face the film is stress free. The stress in the cracked film can be found by considering a series of free body diagrams for different values of x. This gives:

$$
\sigma_x^f = \frac{1}{h}\int_0^x \tau dx \Rightarrow \tag{3.14}
$$

$$
\begin{aligned}
\sigma_x^f &= \tau\frac{x}{h}, \quad (x < L_{slip}) \\
\sigma_z^f &= \sigma_f, \quad (z > L_{slip})
\end{aligned} \tag{3.15}
$$

Where x is the distance from the crack. L_{slip} is the slip length, that is the length necessary to "build up" the film stress σ^f, see figure 3.3. Enforcing equilibrium in the film gives a relation for the slip length

$$
L_{slip} = \frac{\sigma h}{\tau} \tag{3.16}
$$

For the shear lag case, minimum or saturation crack spacing $L_{saturation}$ is typically determined to be the order $L_{slip} < L_{saturation} < 2L_{slip}$. This is because crack spacing larger than $2L_{saturation}$ leaves segments of film which satisfies the cracking condition. On the other hand, for small crack spacings smaller than $L_{saturation}$ the critical crack condition is not satisfied in this range. Using that $\tau_y = \frac{\sigma_y}{\sqrt{3}}$ gives the following condition for the crack spacing

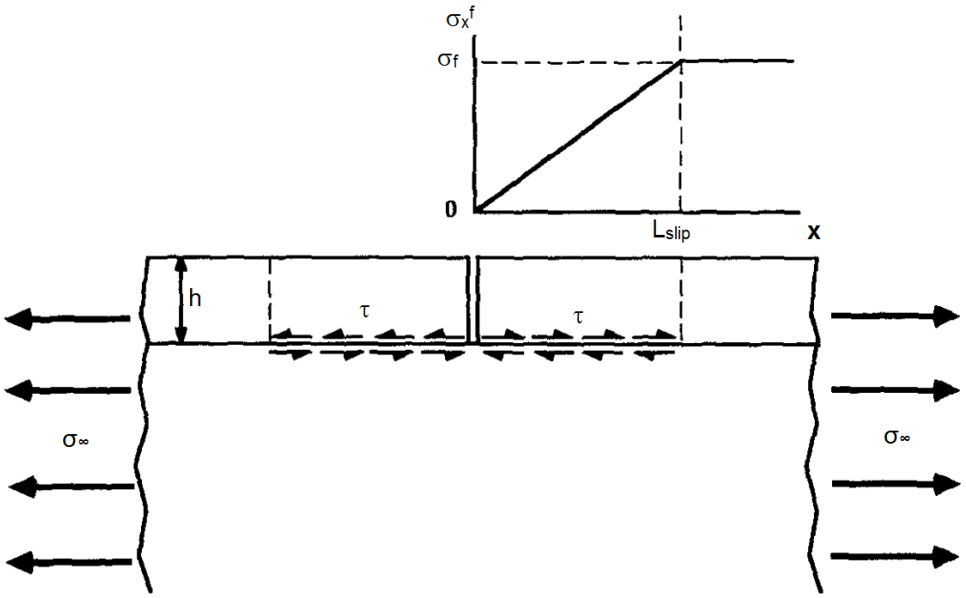

Figure 3.3: An illustration of the shear lag behaviour

for a yielding substrate [14] (interface)

$$\sqrt{3}\frac{\sigma_f}{\sigma_y} < \frac{l_{saturation}}{h} < 2\sqrt{3}\frac{\sigma_f}{\sigma_y} \tag{3.17}$$

Agrawal an Raj [15] assumes that the shear stress transferring the load to the substrate has a sinusoidal distribution instead.

$$\tau = \hat{\tau_y} \sin \frac{2\pi x}{\hat{\lambda}}, \quad 0 \leq x \leq \frac{\hat{\lambda}}{2} \tag{3.18}$$

Where $\hat{\lambda}$ is the wave length for the sine function in equation 3.18. The relation between $\hat{\lambda}$ and the slip length $l_{slip,agrawal}$ is $\hat{\lambda} = 2l_{slip,agrawal}$. Using this expression in equation 3.14 gives the following expression for the shear lag crack spacing

$$\pi\sqrt{3}\frac{\sigma_f}{\sigma_y} < \frac{l_{saturation}}{h} < 2\pi\sqrt{3}\frac{\sigma_f}{\sigma_y} \tag{3.19}$$

3.2 Comparison

The plot in figure 3.4 shows a comparison of the crack spacing as a function of normalised film stress $\frac{\sigma^2 h}{\Gamma_f E_f}$. For comparison, all the plots are an elastic homogenous system. For a fixed value of the film toughness, Γ_f, figure 3.4

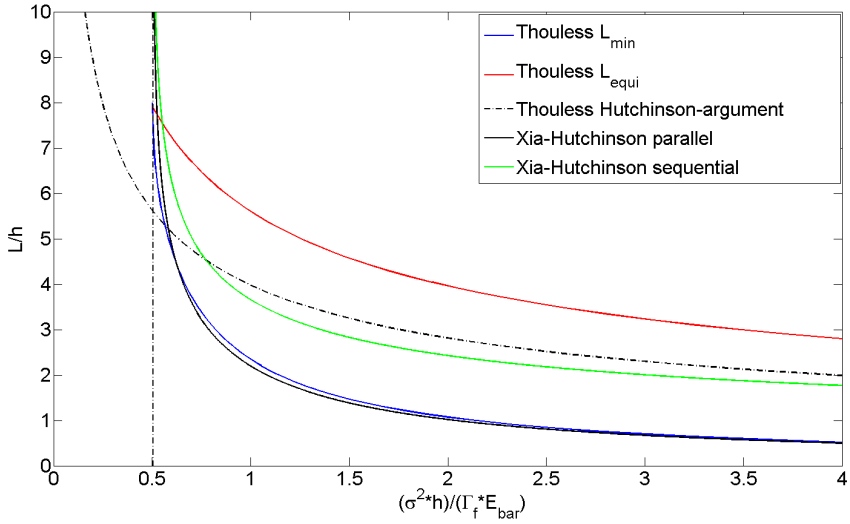

Figure 3.4: Comparison of expression for crack interaction

shows the predicted crack spacing as a function of the normalised film stress. For a given film stress σ, the figure shows the crack spacing given by the various models. The model by [11] dictates the lowest crack spacing. This spacing is given by the expression for the energy release rate for an array of cracks. The crack spacing given by [13] is based on an argument that the equilibrium crack spacing is given by the spacing which minimises the energy in the system. The argument accounts for the sequential propagation of cracks, that a new set of crack will form between existing cracks when the film stress is increased. This argument, equation 3.10, gives a higher spacing that the minimal possible spacing given by equation 3.3. Intermediate to these two crack spacings is the argument for the energy release rate for sequential crack propagation presented by [5]. This argument is presented by two curves. One for equation 3.5 which is the argument from equation 3.4 used on equation 3.2. And one calculated from equation 3.13. These two

curves should be equal but this is not quite the case. The reason for this is not clear, but a reason might be that equation 3.5 is based on equation 3.2 which is not an exact solution. The two expressions giving the crack spacing for a parallel array, equation 3.3 and equation 3.12 are nearly coincident as expected. The vertical dash-dot line indicates the critical normalised stress for a single channelling crack. All the models except equation 3.13 either crosses the line or are very close to the line at $L/h = 8$ which is the spacing at which the cracks do not interact.

For a given crack spacing and normalised film stress, being above and left to the lines would indicate crack propagation.

Chapter 4

Radial cracks patterns from indentations

4.1 Case description

A case of special interest is the one of radial cracks spreading from an indentation crater as seen on figure 4.2. The figure is a picture of a Rockwell C indentation into an aluminium oxide film. A Rockwell C indentation is a standard hardness measurement device in most material laboratories [17]. Equipment used to determine the fracture toughness for thin film is typically micro- or nano indentation equipment [18, 19]. Being able to perform a reliable test on a standard Rockwell indenter would greatly simplify these tests. Also, a Rockwell indentation is a standard method to evaluate the adhesion of the deposited films [20]. The analysis is analogous to the introductory work done by Jensen [21]. The object is to determine the fracture toughness of the deposited film. This is done by linking the stresses in the film to the theoretical models for steady state crack growth described in chapter 3. The models presented is for uniaxial stress in the film. For the current analysis, it is assumed that the models can also be implemented to the axisymmetric stress state present in the vicinity of the indentation crater.

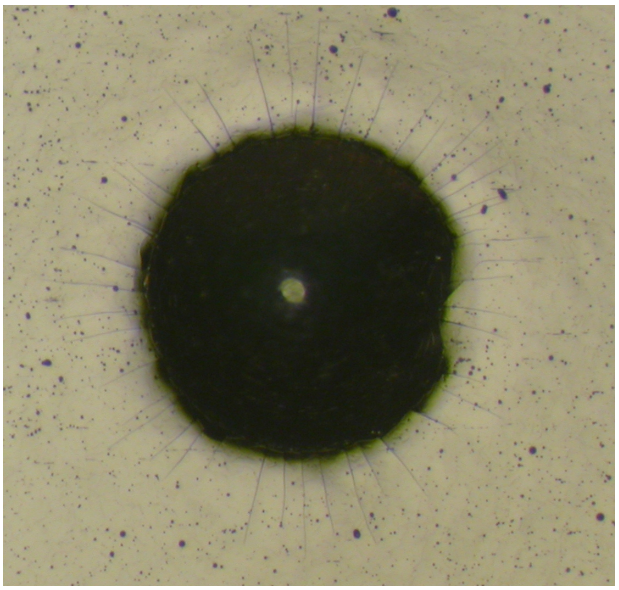

Figure 4.1: Radial crack from Rockwell C indentation in an Al_2O_3 - stainelss steel 316 L system

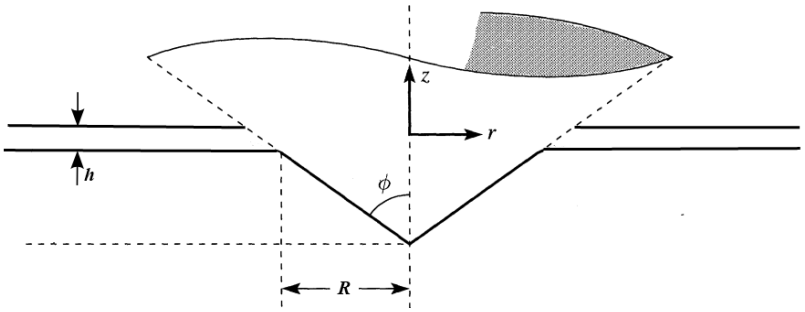

Figure 4.2: Geometry of analysed system

4.2 Determining film stresses

Firstly, an expression for the circumferential stresses is needed. It is assumed that the film thickness h is very small compared to the radius of the indentation crater R and the substrate thickness H. Under this assumption the following expression can be used

$$\sigma_{\theta\theta}(r) = \frac{E}{1-\nu^2}\left(\frac{u(r)}{r} + \nu\frac{du(r)}{dr}\right) \tag{4.1}$$

Where $u(r)$ is the radial displacement of the substrate at the interface. The displacement u is a function of r, the radial distance from the indentation centre. Two properties follow from the assumption $h \ll R$ and enables the use of the expression in equation 4.1 to describe the circumferential stress. Firstly, when the film is thin compared to the indentation radius and substrate thickness it is a reasonable assumption that the displacement of the film equals the displacements of the substrate without the film. Secondly, the contribution to the elastic energy in the film caused by bending can be ignored [22]. Equation 4.1 determines the film stresses from the substrate displacements. This makes the method useful for systems with dissimilar stiffness for film and substrate. If the circumferential strains $\epsilon_{\theta\theta}$ are available the film circumferential stress can be determined directly. if there is no elastic mismatch between film and substrate, results for $\sigma_{\theta\theta}$ can also be used if available.

A first approximation for $u(r)$ is found in [22].

$$\ln\left(\frac{u(r)}{R}\right) = b_0 + b_1\frac{r}{R} + b_2\left(\frac{r}{R}\right)^2 + b_3\left(\frac{r}{R}\right)^3 \tag{4.2}$$

The coefficients $b_0 \ldots b_3$ are in [22] tabulated for various values of yield stress, σ_y, and hardening coefficient, n, in a Ramberg-Osgood true stress-logarithmic strain curve in uniaxial tension

$$\tilde{\epsilon} = \frac{\tilde{\sigma}}{E} + \frac{3}{7}\frac{\sigma_y}{E}\left(\frac{\tilde{\sigma}}{\sigma_y}\right)^{1/N} \tag{4.3}$$

Using common values for σ_y and n for stainless steel 316L the best values tabulated in [22] can be found in table 4.1. The circumferential stress determined using equation 4.1 and equation 4.2 and the values for $b_0 \ldots b_3$ in table 4.1 can be seen in figure 4.3. The indentation edge at $r = R$ is

N	$\frac{\sigma_y}{E_s}$	b_0	b_1	b_2	b_3
0,1	0,0025	2,0424	-5,3558	1,1811	-0,0961

Table 4.1: Values for $b_0 \dots b_3$ used in the analysis

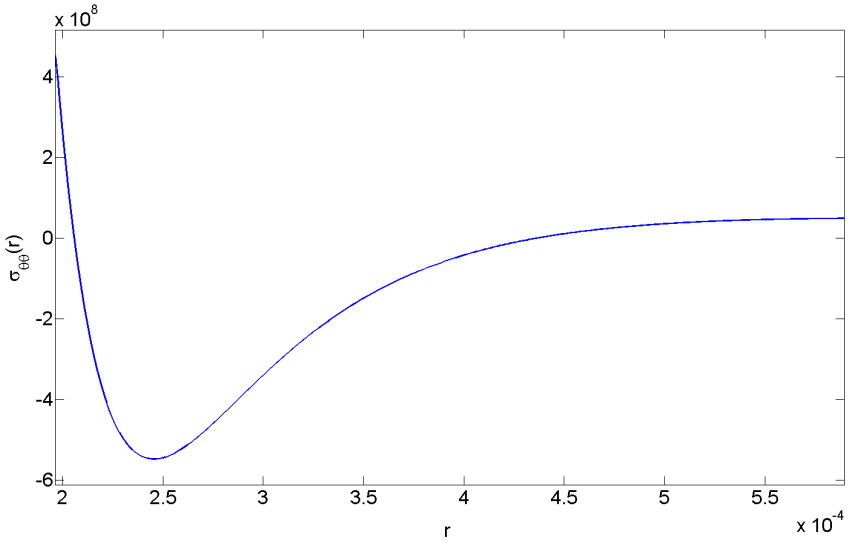

Figure 4.3: $\sigma_{\theta\theta}$ calculated on base of equation 4.2

the left edge of the plot. The plot shows that $\sigma_{\theta\theta}$ very quickly drops to be negative in the range $1,04 \lesssim r/R \lesssim 2,22$ which means that, according to this model, $\sigma_{\theta\theta}$ is negative in the entire range for crack growth in the current case. This is clearly unrealistic and [22] also writes that the expression in equation 4.2 is only valid for $2 \leq r/R \leq 6$. This means that this expression is not very well suited as a first guess for the displacements.

4.2.1 Residual stresses

Residual stress is typically of great importance when considering thin films. Residual stresses can for instance come from the mismatch in coefficients of thermal expansion for the film and substrate. When the film-substrate system is cooled down after manufacturing, large residual stresses can occur. The residual stresses can be in the GPa size range [22]. However, for the

Al_2O_3 film considered here, the residual stresses were measured with a wafer bending test on two Si wafers. The stress was measured to be $2MPa$ to $-34MPa$ respectively which is around the precision for the used method and the film is considered stress free, see section 4.4.

4.3 Determining film properties

The fracture toughness of the film can evaluated using the fracture criterion

$$G_{ss} = \Gamma_f \tag{4.4}$$

Where G_{ss} is the steady-state energy release rate and Γ_f is the fracture toughness of the coating.

The models for the propagation of channelling cracks in chapter 3 can all be presented in the form

$$\frac{L}{h} = F\left(h, \sigma(r), \bar{E}, \Gamma_f\right) \tag{4.5}$$

$\bar{E}$, L/h and h are known values in this analysis. The film stress can generally consist of two components. The first component is the circumferential stress caused by indentation, $\sigma_{\theta\theta}(r)$ and the second component is the equi-biaxial residual stress σ_0 giving $\sigma(r) = \sigma_0 + \sigma_{\theta\theta}(r)$. Unknown quantities in this analysis are the film toughness Γ_f and the residual stress.

The expression in equation 4.5 can the be written for two values of L/h and $\sigma(r)$. One for the crack initiation at the edge of the indentation crater and one for the arresting of crack growth at $r = R + a$

$$\begin{aligned} \frac{L_0}{h} &= F\left(h, \sigma(r = R), \bar{E}, \Gamma_f\right) \\ &\quad \text{and} \\ \frac{L_1}{h} &= F\left(h, \sigma(r = R + a), \bar{E}, \Gamma_f\right) \end{aligned} \tag{4.6}$$

With these two equations, two unknown quantities can be determined, the fracture toughness Γ_f and the residual stress σ_0. Because of the lack of a reliable expression for $\sigma_{\theta\theta}(r)$ an actual determination of Γ_f is not carried through.

4.3.1 Crack regimes as function of residual stress

When cracking has been initiated at the indentation edge, the propagation of cracks may be in one of three regimes depending on the residual stress.

- For no residual stress, for small compressive stresses and for tensile residual stresses below a critical value, the cracks will arrest some distance from the indenter when the circumferential stress drops below the value defined by the crack spacing model showed in figure 3.4. This is the regime seen in figure 4.2. The critical value is given by the driving force for a single crack, equation 2.3

$$\sigma_{0,critical} = \sqrt{\frac{\Gamma_f \bar{E}_f}{1,976h}} \tag{4.7}$$

- If the residual stresses are higher than $\sigma_{0,critical}$ the cracks will not arrest and the film suffers complete failure by unlimited channelling cracking.

- For compressive stresses of high magnitude, the film stresses may not become high enough to initiate crack growth and no radial crack will form.

The three different regimes are sketched on figure 4.4. for illustrative reasons, only the crack criteria from equation 3.13 is included in the figure.

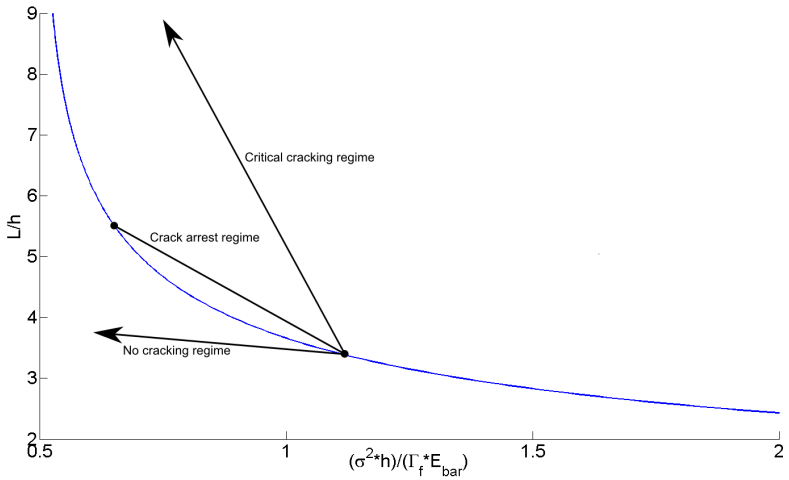

Figure 4.4: Skecth of different cracking regimes

4.4 Film data

The data for the Al_2O_3 film analysed are listed in table 4.2

$\frac{E_{film}}{1-\nu^2}$	h	R	σ_0
$[Gpa]$	$[\mu m]$	$[\mu m]$	$[Mpa]$
213 ± 40	4,1	197	-34 – +2

Table 4.2: Film values used in the analysis

The crack pattern can be seen in mode detail in figure 4.5. As seen in figure 4.5 the crack pattern is not completely homogenous. The crack distances and crack lengths wary significantly. It is difficult to recognise any pattern in the fluctuations. If every second crack was significantly shorter it would indicate that the cracks has developed sequentially. Then the long cracks would have developed first and the shorter cracks would have developed when the load was increased. The reason for this is that the "original" cracks would shield the new cracks, decreasing the driving force [5].

As the pictures does not indicate any clear trend for the crack spacing and crack length, mean values are used in this preliminary study. The mean values for L_0, L_1 and h will be used. The mean values are listed in

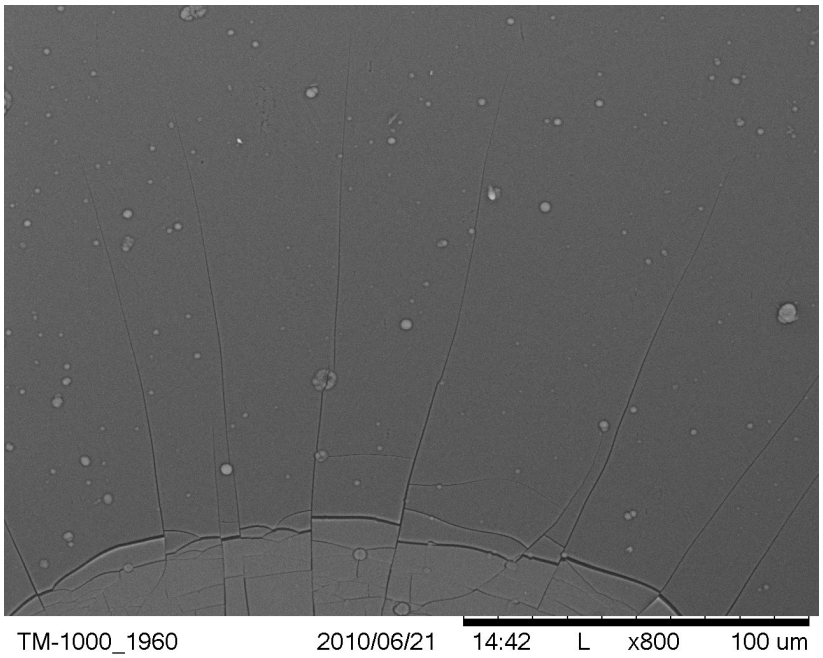

Figure 4.5: Crack pattern in Al_2O_3 film

table 4.3. The Dundurs' parameter α for elastic mismatch can calculated

L_0	$\frac{L_0}{h}$	L_1	$\frac{L_0}{h}$	a
$[\mu m]$	$[-]$	$[\mu m]$	$[-]$	$[\mu m]$
28	6,9	43	10,6	126

Table 4.3: Mean values for L_0, L_1 and a

from equation 2.5. The Poisson's ratio for the film is not known, it is estimated to $\nu_{film} = 0,3$. α is calculated to

$$\alpha = -0.04 \tag{4.8}$$

The results yields that the elastic mismatch can be ignored for the current analysis.

4.5 Issues for further investigation

4.5.1 Indenter friction

Another issue which must be considered if the analysis is to be used for determining the residual stress in the film. Begley et. al. [23] has analysed the mechanical behaviour of a DLC film on a steel substrate indented with a spherical indenter. They showed that the radial strain under the indenter and at the indentation edge is very sensitive to changes in the coefficient of friction between the indenter and the film. Their results for the radial strain can be seen in figure 4.6. When the coefficient of friction mu is lower

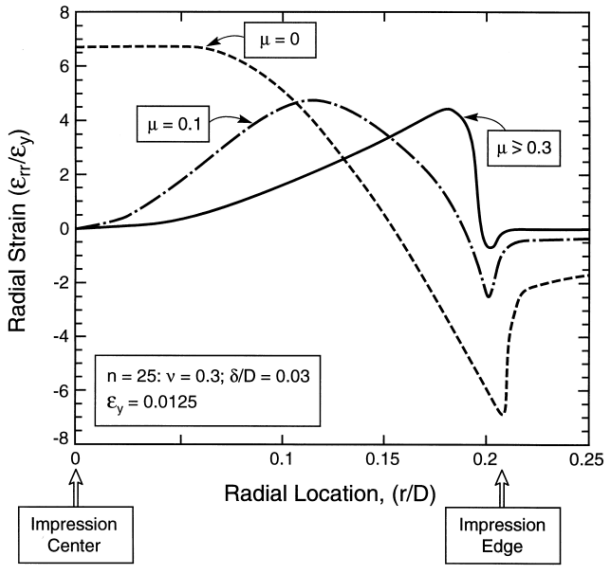

Figure 4.6: Radial strain at different coefficients of friction, [23]

than 0,3 then ϵ_{rr} is very sensitive to friction. When $\mu \geq 0.3$ slip between the indenter and film is prevented. This indicates that to accurately describe the strain and stresses at or near the indentation edge, the friction between indenter and indented material must be examined thoroughly. Begley et. al. describes that μ can be determined by examining the pile-up at the indentation edge. This require detailed knowledge of the plastic properties of the indented material since the yield strength and hardening coefficient also effects the pile-up [24, 23, 25].

4.5.2 Film stress model

It is clear from the above that a precise expression for the circumferential stresses is needed. Work is in progress to use stresses from an FEM model of a Rockwell indentation made by Søren Steffensen. The FEM model is an elastic-plastic analysis including contact and large displacement which simulates a Rockwell C indentation. As an introductory method to validate the FEM results, the results for the radial displacement u are compared to the results given by [22]. The FEM analysis is performed for a Young's modulus $E = 180GPa$ and plastic properties are chosen to be $N = 0,01$ and $\frac{\sigma_y}{E} = 0,005$ in the Ramberg-Osgood relation from equation 4.3. The function in equation 4.2 is given for these plastic values and a comparison can be made. Figure 4.7 shows the deformed surface from the FEM

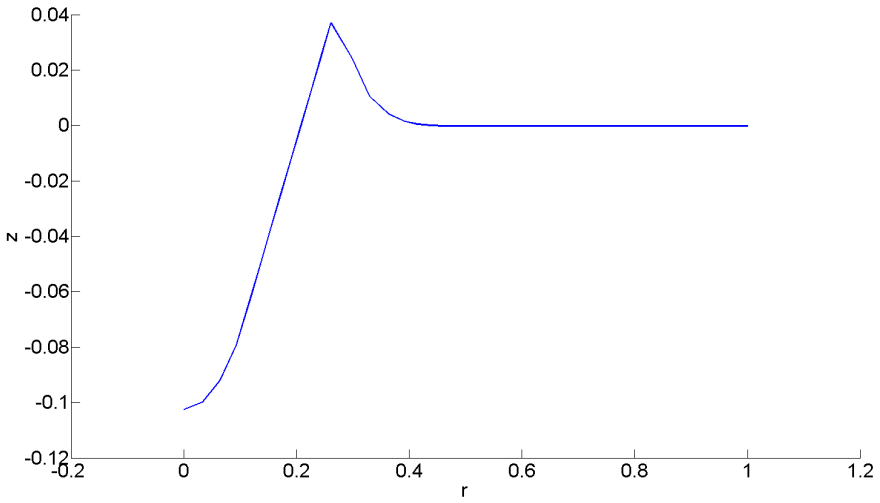

Figure 4.7: surface profile of the indented surface from FEM analysis

analysis. The indentation edge is clearly seen at $r = 261\mu m$. Some pile-up can also be seen.

The radial displacements $u(r)$ for the FEM analysis and equation 4.2 can be seen in figure 4.8. The plot is shown for $2 > r/R > 4$ since equation 4.2 is valid only for $2 > r/R > 5$ and the FEM results are given only for $r/R > 4$. The figure shows that the two sets of results are far from equal.

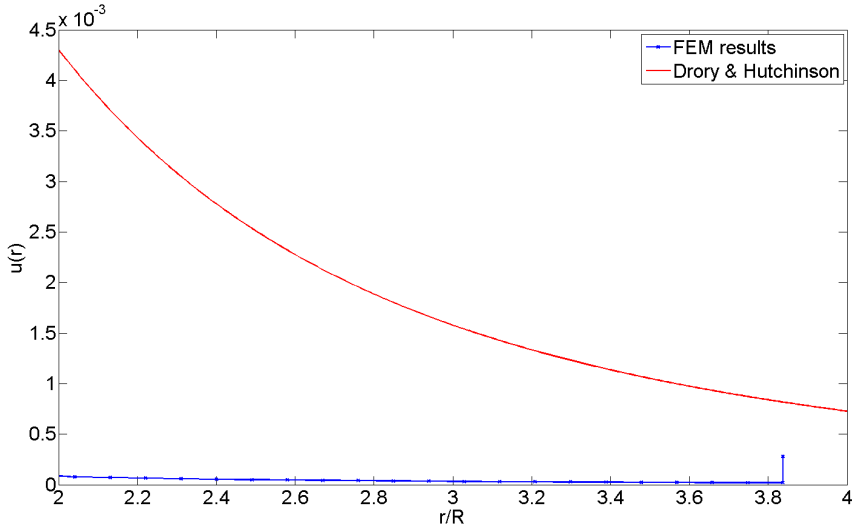

Figure 4.8: Comparison of radial surface displacements from FEM analysis and equation 4.2

The FEM model used has been thoroughly tested and validated. Such a large difference does require further investigation which has not been carried out at current time.

Chapter 5

Conclusion and future work

The general topic in the ongoing project is investigation of the fracture mechanical properties of thin films and linking these to wear properties for the coated systems. Basic mechanisms in thin film fracture has been described. A number of models describing the propagation and interaction of cracks in thin films has been investigated and explained. The mechanisms described includes crack interaction, yielding substrate and elastic mismatch between the film and substrate. An approach has been set up to determine fracture toughness and residual stress in a thin film by studying the density and propagation of radial crack from a standard Rockwell indentation. Issues to consider when developing this model to a reliable method is described.

5.1 Future work

A number of topics need further investigation before results and conclusions can be made from these. Other crack types than the radial stresses seen in figure 4.2 has been observed, see figure 5.1.

The circumferential crack case is being investigated with a number of approaches. One approach is to treat the film-substrate system as a beam or plate resting on an elastic or yielding foundation. When loaded by an indentation, the film cracks where tensile stresses at the surface has a maximum. This maximum may be determined by bending stress and in-plane stresses in the film. This plate-bending approach has been explored by [26], [27] and [28]. Another approach when considering circumferential cracks is to assume that the substrate yields beneath the indenter and the circum-

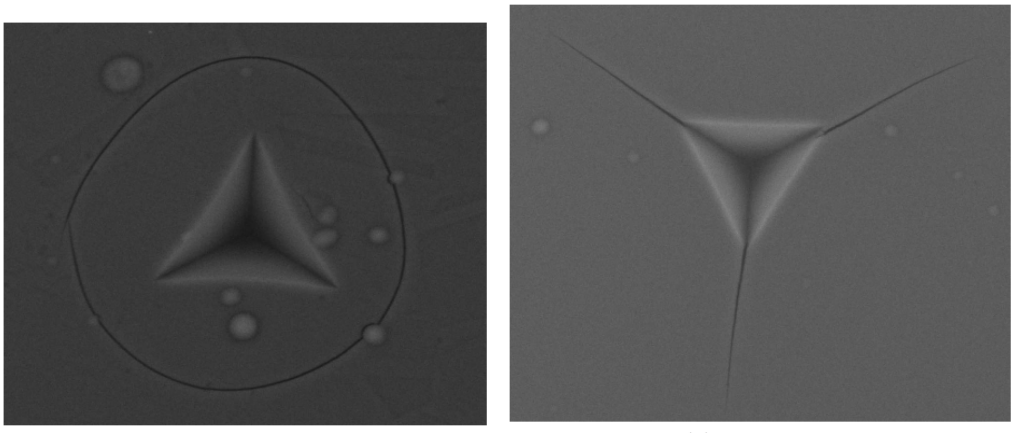

(a) circumferential crack (b) Radial crack

Figure 5.1: Two crack types detected during indentation with a Berkovich indenter

ferential crack forms at the edge of the plastic zone. This approach has been used by [29] and [30] in combination with finite element simulation and nano-indentation response results.

Wear is another key topic in this research project. A focus point in the project is to link fracture mechanical properties to the wear properties and wear mechanisms of the films. The fracture mechanisms taking place is tightly connected to the kind of load applied to the coating. The load scenarios relevant in the project is considered to be sliding contact and rolling-sliding contact. [31], [32] and [33] have visually investigated wear surfaces of DLC coatings under sliding and rolling sliding load by the use of focused ion beam cutting and have set up fracture mechanical models for the surface wear. Sliding wear is also investigated by [34], [35] and [36]. These references in generally combines contact stresses and friction forces with models for the initiation and propagation of microcracks in the wake of the load.

Bibliography

[1] J.W. Hutchinson. Mechanics of thin films and multilayers: Course notes. Course notes, DTU, `http://www.seas.harvard.edu/hutchinson/papers/462-5.pdf`, October 1996.

[2] Z. Xia and J.W. Hutchinson. Crack patterns in thin films. *Journal of the Mechanics and Physics of Solids*, 48(6-7):1107–1131, 2000.

[3] T. Nakamura and S. Kamath. Three-dimensional effects in thin film fracture mechanics. *Mechanics of Materials*, 13(1):67–77, March 1992.

[4] J. Ambrico and M.R. Begley. The role of initial flaw size, elastic compliance and plasticity in channel cracking of thin films. *Thin Solid Films*, 419(1-2s):144–153, 2002.

[5] J.W. Hutchinson and Z. Suo. Mixed mode cracking in layered materials. *Advances in applied mechanics*, 29(63):191, 1992.

[6] H. Tada, P.C. Paris, and G.R. Irwin. *The Stress Analysis of Cracks Handbook*. ASME, 3 edition, 2000.

[7] J. Dundurs. Edge-bonded dissimilar orthogonal elastic wedges under normal and shear loading. *Journal of Applied Mechanics*, 36:650–652, 1969.

[8] Siegfried Schmauder and Markus Meyer. Correlation between Dundurs' parameters and elastic constants. *Zeitschrift für Metallkunde*, 83:524–527, 1992.

[9] J.L. Beuth. Cracking of thin bonded films in residual tension. *International Journal of Solids and Structures*, 29(13):1657–1675, 1992.

[10] A.R. Zak and M.L. Williams. Crack point stress singularities at a bi-material interface. *Journal of Applied Mechanics*, 30:142–143, 1963.

[11] M.D. Thouless. Crack spacing in brittle films on elastic substrates. *Journal of the American Ceramic Society*, 73(7):2144–2146, 1990.

[12] F. Delannay and P. Warren. On crack interaction and crack density in strain-induced cracking of brittle films on ductile substrates. *Acta metallurgica et materialia*, 39(6):1061–1072, 1991.

[13] M.D. Thouless, E. Olsson, and A. Gupta. Cracking of brittle films on elastic substrates. *Acta Metallurgica et Materialia*, 40(6):1287–1292, 1992.

[14] M. Hu and A. Evans. The cracking and decohesion of thin films on ductile substrates. *Acta Metallurgica*, 37(3):917–925, March 1989.

[15] D.C. Agrawal and R. Raj. Measurement of the ultimate shear strength of a metal-ceramic interface. *Acta Metallurgica*, 37(4):1265–1270, 1989.

[16] J.L. Beuth and N.W. Klingbeil. Cracking of thin films bonded by elastic-plastic substrates. *Science*, 44(9):1411–1428, 1996.

[17] Conrad Vogel, Celia Juhl, and Ernst Maahn. *Metallurgi for Ingeniører*. Polyteknisk Forlag, 9 edition, 2001.

[18] J. Jungk, B. Boyce, T. Buchheit, T. Friedmann, D. Yang, and W. Gerberich. Indentation fracture toughness and acoustic energy release in tetrahedral amorphous carbon diamond-like thin films. *Acta Materialia*, 54(15):4043–4052, September 2006.

[19] Herzl Chai. Indentation-induced subsurface tunnelling cracks as a means for evaluating fracture toughness of brittle coatings. *International Journal of Fracture*, 158(1):15–26, jun 2009.

[20] Verein Deutscher Ingenieure, `http://www.vdi.de/401.0.html?&L=1&tx_vdirili_pi2%5BshowUID%5D=90478`. *VDI 3198: Guideline: Coating (CVD, PVD) of cold forging tools*, September 2003.

[21] H.M. Jensen. Indentation cracking of brittle solids. In B. L. Karihaloo, Y. W. Mai, M.I. Ripley, and R.O. Ritchie, editors, *Advances in Fracture Research*, pages 2423–2431. Pergamon, 1997.

[22] M.D. Drory and J.W. Hutchinson. Measurement of the adhesion of a brittle film on a ductile substrate by indentation. *Proceedings of the Royal Society A: Mathematical, Physical and Engineering Sciences*, 452(1953):2319–2341, Oct 1996.

[23] M.R. Begley, A.G. Evans, and J.W. Hutchinson. Spherical impression of thin elastic films on elastic-plastic substrates. *International Journal of Solids*, pages 1662–1677, 1999.

[24] B. Taljat and G.M. Pharr. Development of pile-up during spherical indentation of elasticŰplastic solids. *International Journal of Solids and Structures*, 41(14):3891–3904, July 2004.

[25] R. Hill, B. Storakers, and A.B. Zdunek. A theoretical study of the brinell hardness test. *Proceedings of the Royal Society A: Mathematical, Physical and Engineering Sciences*, 423(1865):301–330, June 1989.

[26] M.R. McGurk, H.W. Chandler, P.C. Twigg, and T.F. Page. Modelling the hardness response of coated systems: the plate bending approach. *Surface and Coatings Technology*, 68-69:576–581, December 1994.

[27] M.R. McGurk and T.F. Page. Exploration of the plate bending model for predicting the hardness response of coated systems. *Surface and Coatings Technology*, 92:87–95, 1997.

[28] P. Ramsey. Modelling the contact response of coated systems. *Surface and Coatings Technology*, 49(1-3):504–509, December 1991.

[29] D.F. Bahr, C.L. Woodcock, M. Pang, K.D. Weaver, and N.R. Moody. Indentation induced film fracture in hard film Ű soft substrate systems. *International Journal of Fracture*, 119/120(4-2):339–349, 2003.

[30] M. Pang and D.F. Bahr. Thin-film fracture during nanoindentation of a titanium oxide film-titanium system. *Journal of Materials Research*, 16(9):2634–2643, 2001.

[31] C. Mercer, A.G. Evans, N. Yao, S. Allameh, and C.V. Cooper. Material removal on lubricated steel gears with W-DLC-coated surfaces. *Surface and Coatings Technology*, 173(2-3):122–129, August 2003.

[32] R. Wang, C. Mercer, A.G. Evans, C.V. Cooper, and H.K. Yoon. Delamination and spalling of diamond-like-carbon tribological surfaces. *Diamond and Related Materials*, 11(10):1797–1803, October 2002.

[33] N. Yao, A.G. Evans, and C.V. Cooper. Wear mechanism operating in W-DLC coatings in contact with machined steel surfaces. *Surface and Coatings Technology*, 179(2-3):306–313, February 2004.

[34] A Bower and N Fleck. Brittle fracture under a sliding line contact. *Journal of the Mechanics and Physics of Solids*, 42(9):1375–1396, Sep 1994.

[35] J. Malzbender and G. de With. Modeling of the fracture of a coating under sliding indentation. *Wear*, 239(1):21–26, April 2000.

[36] R.B. King and T.C. O'sullivan. Sliding contact stresses in a two-dimensional layered elastic half-space. *International Journal of Solids and Structures*, 23(5):581–597, 1987.

Mads Krabbe, Crack Mechanisms and Crack Interaction in Thin Films, 2012

Department of Engineering
Aarhus University
Edison, Finlandsgade 22
8200 Aarhus N
Denmark

Tel.: +45 4189 3000